

Strong enhancement of s -wave superconductivity near a quantum critical point of $\text{Ca}_3\text{Ir}_4\text{Sn}_{13}$ P. K. Biswas,¹ Z. Guguchia,¹ R. Khasanov,¹ M. Chinotti,^{1,*} L. Li,^{2,†} Kefeng Wang,^{2,‡} C. Petrovic,² and E. Morenzi^{1,§}¹Laboratory for Muon Spin Spectroscopy, Paul Scherrer Institute, CH-5232 Villigen PSI, Switzerland²Condensed Matter Physics and Materials Science Department, Brookhaven National Laboratory, Upton, New York 11973, USA

(Received 26 June 2015; revised manuscript received 15 September 2015; published 11 November 2015)

We report microscopic studies by muon spin rotation/relaxation as a function of pressure of the $\text{Ca}_3\text{Ir}_4\text{Sn}_{13}$ and $\text{Sr}_3\text{Ir}_4\text{Sn}_{13}$ cubic compounds, which are members of the $(\text{Ca}_{1-x}\text{Sr}_x)_3\text{Ir}_4\text{Sn}_{13}$ system displaying superconductivity and a structural phase transition associated with the formation of a charge density wave (CDW). We find a strong enhancement of the superfluid density and a dramatic increase of the pairing strength above a pressure of ≈ 1.6 GPa, giving direct evidence of the presence of a quantum critical point separating a superconducting phase coexisting with CDW from a pure superconducting phase. The superconducting order parameter in both phases has the same s -wave symmetry. In spite of the conventional phonon-mediated BCS character of the weakly correlated $(\text{Ca}_{1-x}\text{Sr}_x)_3\text{Ir}_4\text{Sn}_{13}$ system, the dependence of the effective superfluid density on the critical temperature puts this compound in the “Uemura” plot close to unconventional superconductors. This system exemplifies that conventional BCS superconductors in the presence of competing orders or multiband structure can also display characteristics of unconventional superconductors.

DOI: [10.1103/PhysRevB.92.195122](https://doi.org/10.1103/PhysRevB.92.195122)

PACS number(s): 74.25.Ha, 74.25.Dw, 74.70.Dd, 76.75.+i

I. INTRODUCTION

The interplay between different electronic ground states is one of the fundamental topics in condensed-matter physics and is very apparent in phase diagrams as a function of doping, pressure, or magnetic fields, resulting in various forms of coexistence, cooperation, or competition of the order parameters [1–4]. Particularly interesting are the regions at phase boundaries or at quantum critical points (QCPs) where different quantum states meet [5]. Very often, magnetism and superconductivity are involved and, in spite of diverse structural and physical properties, many compounds show characteristic phase diagrams where superconductivity is found in the vicinity of electronic instabilities of magnetic (mainly antiferromagnetic) origin. In this case, spin fluctuations are predominantly considered at the heart of the mechanisms leading to pairing, and superconductivity is unconventional. Less common is the case where the electronic instability is linked to the formation of a charge density wave (CDW), which is based on the same electron-phonon interaction found in conventional superconductors.

Ternary intermetallic stannide compounds such as $R_3T_4\text{Sn}_{13}$, where $R = \text{La, Ca, Sr}$ and $T = \text{Ir, Rh}$ [6,7], are of particular interest because they exhibit many physical properties such as superconductivity, magnetic or charge order, and structural instabilities. The quasikutteridite cubic superconductor $(\text{Ca,Sr})_3\text{Ir}_4\text{Sn}_{13}$ and the related $(\text{Ca,Sr})_3\text{Rh}_4\text{Sn}_{13}$ have recently attracted attention because of the presence of a pressure-induced structural phase transition at a temperature T^* , the possible coexistence of superconducting and

charge density wave states, and a putative quantum critical point [8–16]. The role and interplay of these degrees of freedom remain a central issue also in many unconventional superconductors, as demonstrated by the recent observation of CDW in $\text{HgBa}_2\text{CuO}_{4+\delta}$ [17] and of competition between superconductivity and charge order in $\text{YBa}_2\text{Cu}_3\text{O}_{6.67}$ [18]. In $(\text{Ca}_{1-x}\text{Sr}_x)_3\text{Ir}_4\text{Sn}_{13}$, the phase transition was found following the observation of an anomaly in temperature-dependent resistivity and susceptibility measurements at $T^* \simeq 147$ K and $T^* \simeq 33$ K in $\text{Sr}_3\text{Ir}_4\text{Sn}_{13}$ and $\text{Ca}_3\text{Ir}_4\text{Sn}_{13}$, respectively. Initially, the anomaly was attributed to ferromagnetic spin fluctuations, coexisting and possibly enhancing the superconductivity appearing at lower temperature $T_c \simeq 5$ K and $T_c \simeq 7$ K in $\text{Sr}_3\text{Ir}_4\text{Sn}_{13}$ and $\text{Ca}_3\text{Ir}_4\text{Sn}_{13}$, respectively [19]. Later, single-crystal x-ray diffraction and neutron-scattering studies showed that the anomaly in $\text{Sr}_3\text{Ir}_4\text{Sn}_{13}$ and $\text{Ca}_3\text{Ir}_4\text{Sn}_{13}$ is produced by a second-order structural transition at T^* [8,10].

Various physical quantities from transport and magnetization measurements suggest that the transition is associated with a charge density wave transition involving the conduction electrons system [8]. Measurements of Hall and Seebeck coefficients and ^{119}Sn nuclear magnetic resonance (NMR) indicate a decrease of the carrier density and significant Fermi-surface reconstruction with change of sign of the Hall coefficient at T^* in $\text{Ca}_3\text{Ir}_4\text{Sn}_{13}$ and $\text{Sr}_3\text{Ir}_4\text{Sn}_{13}$ [11–13]. Optical spectroscopy reveals the formation of a partial energy gap at the Fermi surface associated with the structural phase transition [14].

μSR measurements of the two end compounds $\text{Ca}_3\text{Ir}_4\text{Sn}_{13}$ and the isoelectronic sister compound $\text{Sr}_3\text{Ir}_4\text{Sn}_{13}$ at ambient pressure did not find any sign of magnetic ordering or weak magnetism of static or dynamic origin [20–22] and found BCS-like superconductivity with s -wave symmetry and a $\Delta(0)/(k_B T_c)$ ratio typical of strong coupling similar to other $R_3T_4\text{Sn}_{13}$ compounds [23,24]. Since the atomic size of Ca is smaller than that of Sr, the substitution of Ca on the Sr site corresponds to applying a positive pressure of about 5.2 GPa, which reduces T^* . This behavior continues in $(\text{Ca}_{1-x}\text{Sr}_x)_3\text{Ir}_4\text{Sn}_{13}$ for external pressure. At the same time, an

*Current address: Laboratory for Solid State Physics, ETH Zurich, CH-8093 Zurich, Switzerland.

†Current address: Key Laboratory of Materials Physics, Institute of Solid State Physics, Chinese Academy of Sciences, Hefei 230031, China.

‡Current address: Department of Physics, University of Maryland, College Park, Maryland 20742-4111, USA.

§Corresponding author: elvezio.morenzi@psi.ch

increase of T_c with increasing pressure has been observed so that, under hydrostatic pressure, the T_c of $\text{Ca}_3\text{Ir}_4\text{Sn}_{13}$ reaches 8.9 K at ~ 4.0 GPa and then falls for higher pressures [8]. A linear extrapolation of the $T^*(p)$ dependence to $T^* = 0$ predicts a structural/CDW quantum critical point at ≈ 1.8 GPa. Note, however, that this value has been extracted from measurements of T^* in the normal state, so that the available data have not given direct evidence of a QCP in the superconducting state.

The increase of T_c with pressure and the concomitant suppression of the T^* point to an intimate interplay between CDW and superconductivity, possibly culminating in a quantum critical point where the CDW is completely suppressed. There is a longstanding question concerning the competition, coexistence, or cooperation between the two electronic states as well as about the role of charge density fluctuations. A CDW opens a gap on part of the Fermi surface and can therefore profoundly modify the microscopic properties and gap structure of the superconductor. The $(\text{Ca}_{1-x}\text{Sr}_x)_3\text{Ir}_4\text{Sn}_{13}$ compound allows one to investigate the questions of competing electronic/structural instabilities, as well as whether these states are separated by a QCP and how the pairing state evolves around such a point.

Here, we use the μSR technique to characterize at a microscopic level the superconducting and magnetic properties in $\text{Ca}_3\text{Ir}_4\text{Sn}_{13}$ and $\text{Sr}_3\text{Ir}_4\text{Sn}_{13}$ as a function of pressure. In particular, from measurements of the inhomogeneous field distribution in the vortex state $p(B)$, we determine the effective magnetic penetration depth $\lambda(T)$ and its temperature and pressure dependence. μSR is a powerful tool to determine the absolute value of $\lambda(T)$ and its dependence on various thermodynamic parameters. The magnetic penetration depth is a fundamental property of the superconducting state, which can be measured to probe the electronic structure of the material and to look for signatures of a QCP. The temperature dependence of λ^{-2} is a measure of the superfluid density $\lambda^{-2} \propto \rho_s \equiv \frac{n_s}{m^*}$ (where n_s is the supercarrier density and m^* is the effective mass), whereas the low-temperature behavior of $\lambda(T)$ reflects the superconducting gap structure. Despite the importance of the evolution of this quantity in understanding the nature of superconductivity, especially around a zero-temperature quantum transition, there are not many measurements on the pressure dependence on λ and only a small number of μSR studies on the effect of pressure have been reported so far [25–27].

Here we observe a pronounced increase of the superfluid density that sets in at a pressure $p_c \approx 1.6$ GPa with a sudden enhancement of the superconducting gap value, indicating that a QCP exists in the superconducting state, leading to a significant enhancement of the superconducting pairing strength when the CDW is suppressed. We find that $\text{Ca}_3\text{Ir}_4\text{Sn}_{13}$ remains a conventional electron-phonon-coupled s -wave superconductor across the quantum phase transition. The strengthening of the superconducting coupling at p_c appears to be related to the phonon softening at the structural quantum critical point. Although a conventional superconductor, the dependence of T_c on superfluid density resembles that of unconventional superconductors when plotted in the so-called Uemura plot. This system exemplifies that conventional BCS superconductors can also display unconventional

features in the presence of competing orders or multiband structure.

II. RESULTS

Single-crystal samples of $\text{Ca}_3\text{Ir}_4\text{Sn}_{13}$ and $\text{Sr}_3\text{Ir}_4\text{Sn}_{13}$ were grown as described in Ref. [13]. Transverse-field (TF) μSR experiments were performed on the general-purpose decay-channel spectrometer (GPD) at the $\mu\text{E}1$ beam line of the Paul Scherrer Institute. High-energy muons ($p_\mu \sim 100$ MeV/c) were implanted in the sample. Forward and backward positron detectors with respect to the initial muon polarization were used for the measurements of the μSR asymmetry time spectrum $A(t)$. The spectra yield information about the superconducting properties. For instance, the average muon spin precession frequency is directly proportional to the average local magnetic field at the muon site and can detect a diamagnetic shift associated with the supercurrents. In the vortex state with a typical field distribution, the precession is damped and the damping is related to the field distribution, which depends on the characteristic length scales of the superconductor [28].

Muon spin rotation (μSR) spectra in the vortex state were taken as a function of increasing temperature by initially field cooling the sample down to 0.3 K in a 50 mT in the case of $\text{Ca}_3\text{Ir}_4\text{Sn}_{13}$ and 30 mT field for $\text{Sr}_3\text{Ir}_4\text{Sn}_{13}$ and for different pressures. Typical statistics for a μSR spectrum were about 5×10^6 positron events in the forward and backward detectors. Several (single-crystal) pieces of the compound were loaded into the cylindrical pressure cell. The sample dimensions were chosen to maximize the filling factor of the pressure cell (diameter 6 mm, height 15 mm). A CuBe piston-cylinder pressure cell was used with Daphne oil as a pressure-transmitting medium for pressures up to 1.1 GPa; from 1.1 GPa and above, MP35N was used. The maximum pressure achieved at low temperature is about 2.2 GPa. The pressure was calibrated by measuring, via ac susceptibility, the superconducting transition of a very small indium plate inserted in the cell. The pressure point at 1.1 GPa was measured with the two different cells to better assess the background contribution arising from muons stopping in the cell walls and check that the use of the two cell materials had no effect on the results. The fraction of the muons stopping in the sample was approximately 50% with the CuBe cell and 40% with the MP35N cell. Resistivity and magnetoresistance measurements to determine $\rho(T)$ and $B_{c2}(T)$ were performed using a PPM Quantum Design instrument. Additional characterization of the samples grown under the same conditions, such as specific heat, Seebeck coefficient, and Hall resistivity, can be found in Ref. [13].

Typical μSR spectra in the normal and superconducting states at a low and a high hydrostatic pressure are shown in Fig. 1. The data were fitted with the equations described in the Supplemental Material to extract the moments of the field distribution probed by the muons thermalized in the sample [28]. The temperature dependence of the spin-depolarization rate σ (proportional to the second moment of the field distribution) of muons stopping in the $\text{Ca}_3\text{Ir}_4\text{Sn}_{13}$ sample and of the average internal field at different hydrostatic

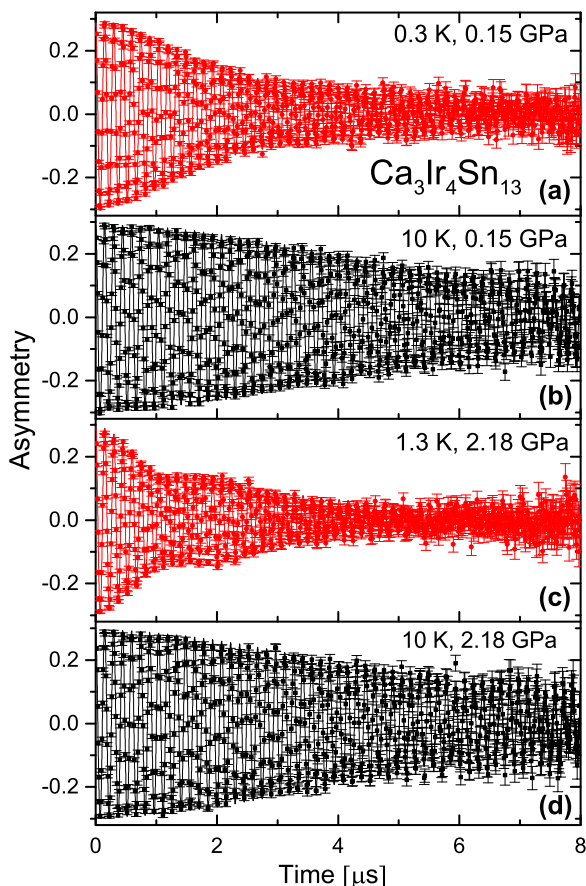


FIG. 1. (Color online) Asymmetry spectra for $\text{Ca}_3\text{Ir}_4\text{Sn}_{13}$ measured (a),(c) below and (b),(d) above T_c and at pressures of (a),(b) 0.15 GPa and (c),(d) 2.18 GPa after cooling the sample in a transverse field (TF) of 50 mT. The increased damping below T_c at shorter times reflects the formation of a vortex lattice and the dephasing of the muon ensemble in the corresponding field distribution. At higher pressure, the damping is more pronounced, reflecting a shorter magnetic penetration depth. The residual damping observed in the normal state is due to the contribution of the nuclear moments in the sample. The solid line is the fits, as described in the Supplemental Material [28], which also take into account the background contribution from the muons stopping in the pressure cell walls.

pressures are shown in Figs. S1 and S2 of the Supplemental Material [28], respectively.

Typically, σ increases from σ_n in the normal state, to $\sigma = \sqrt{\sigma_s^2 + \sigma_n^2}$ below T_c , reflecting the inhomogeneous field distribution due to the decrease of the effective magnetic penetration depth λ or, equivalently, to the increase of the effective superfluid density $\rho_s \equiv n_s/m^*$ when entering the vortex state [$1/\lambda(T)^2 \propto n_s(T)/m^*$, where $n_s(T)$ is the density of supercarriers and m^* is the effective mass]. Figure S2 [28] clearly shows that $\sigma_s(T)$ increases with pressure.

In an isotropic type-II superconductor with a hexagonal Abrikosov vortex lattice described by Ginzburg-Landau theory, the magnetic penetration depth λ is related to σ_s by the equation [29]

$$\sigma_s(T) \mu\text{s}^{-1} = 4.854 \times 10^4 (1 - b) \times [1 + 1.21(1 - \sqrt{b})^3] \lambda(T)^{-2} \text{ nm}^{-2}. \quad (1)$$

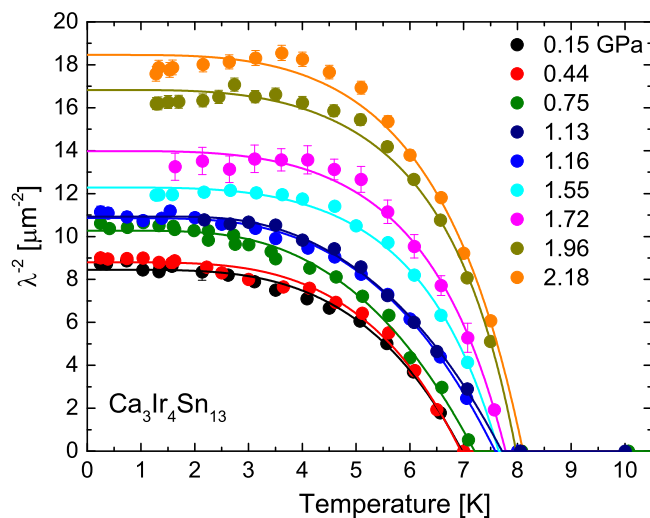


FIG. 2. (Color online) Temperature dependence of the superfluid density in the vortex state of $\text{Ca}_3\text{Ir}_4\text{Sn}_{13}$, measured at various pressures after field cooling in 50 mT. The fit lines were obtained using the procedure explained in the text.

Here, $b = \langle B \rangle / B_{c2}$ is a reduced magnetic field, with $\langle B(T) \rangle$ the first moment of the field distribution determined from the fit (see Supplemental Material and Fig. S1 [28]) and $B_{c2}(T)$ the second critical field determined by magnetoresistance and corrected for the small pressure effects according to Ref. [30]. These terms in Eq. (1) take into account that the intervortex distance decreases with increasing applied field, thus narrowing the field distribution. They are small in our case since in the relevant temperature range, $\langle B \rangle \cong B_{\text{applied}} \ll B_{c2}$.

Figure 2 shows the temperature dependence of $1/\lambda^2$ taken at various pressures. The measurements at 1.13 and 1.16 GPa were performed with the MP35N and the CuBe cell, respectively. The results agree very well, demonstrating the absence of systematic errors related to the cell type. Inspection of the figure clearly shows that the superfluid density increases with pressure and that this increase is more pronounced at pressures $p \gtrsim 1.7$ GPa. For all pressures, there is no pronounced temperature dependence at low temperatures, which is typical for a fully gapped s -wave superconductor, where $\Delta\lambda(T) = \lambda(T) - \lambda(0)$ decays exponentially; we find similar behavior for $\text{Sr}_3\text{Ir}_4\text{Sn}_{13}$. For all investigated pressures, the data can be well fitted using in Eq. (1) the expression for a dirty superconductor with a single s -wave gap [31]:

$$\frac{\rho_s(T)}{\rho_s(0)} = \frac{\lambda^2(0)}{\lambda^2(T)} = \frac{\Delta(T)}{\Delta(0)} \tanh \frac{\Delta(T)}{2k_B T}, \quad (2)$$

where $\Delta(T)$ is the BCS superconducting gap. The dirty character of $\text{Ca}_3\text{Ir}_4\text{Sn}_{13}$ is confirmed by our determination of various normal-state and superconducting parameters, which are presented in the discussion section. A useful parametrization of the BCS gap [32] is given in Ref. [33] by $\Delta(T) = \Delta(0) \tanh\{1.82[1.018(T_c/T - 1)]^{0.51}\}$. Such a parametrization has been found to well represent the temperature dependence at any coupling strength [34]. The fits yield the pressure dependence of the critical temperature T_c , the superfluid density $1/\lambda(0)^2$, and the superconducting gap $\Delta(0)$. The results are

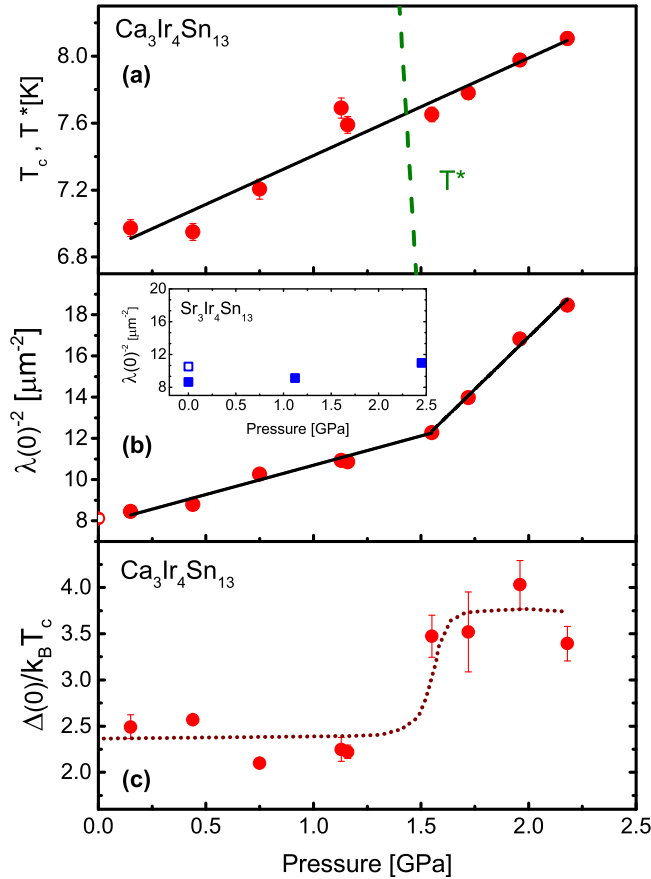


FIG. 3. (Color online) (a) Critical temperature vs applied pressure in $\text{Ca}_3\text{Ir}_4\text{Sn}_{13}$ with linear fit. The dashed line indicates the T^* pressure dependence from [8]. No anomaly is observable around the critical pressure $p_c \approx 1.6$ GPa. (b) Pressure dependence of the superfluid density of $\text{Ca}_3\text{Ir}_4\text{Sn}_{13}$ at $T = 0$, proportional to $\lambda(0)^{-2}$ obtained from the fit shown in Fig. 2. Lines are linear fits in the two pressure regimes below and above the critical pressure. The inset shows the corresponding pressure range for $\text{Sr}_3\text{Ir}_4\text{Sn}_{13}$, which is offset with respect to $\text{Ca}_3\text{Ir}_4\text{Sn}_{13}$ by -5.2 GPa. Open symbols are $p = 0$ data from [21,22]. (c) Gap-to- T_c ratio $R \equiv \Delta(0)/(k_B T_c)$ vs pressure in $\text{Ca}_3\text{Ir}_4\text{Sn}_{13}$. The dashed line is to guide the eyes.

shown in Figs. 3(a)–3(c), respectively. The critical temperature increases almost linearly with increasing pressure. A linear fit yields $dT_c/dp = 0.592(76)$ K/GPa with an intercept at $p = 0$ of 6.79(6) K. The smooth $T_c(p)$ dependence is in sharp contrast to the behavior of the superfluid density and of the gap-to- T_c ratio as a function of pressure, where the changes cannot be simply related to pressure changes in T_c . The dependence of the superfluid density on pressure displays a pronounced change of slope above a pressure $p_c \approx 1.6$ GPa. Above this value, the slope is more than a factor of three higher than below: $d\lambda(0)^{-2}/dp = 2.84(18) \mu\text{m}^{-2}/\text{GPa}$ for $p \leq p_c$ and $d\lambda(0)^{-2}/dp = 10.17(62) \mu\text{m}^{-2}/\text{GPa}$ for $p \geq p_c$. Equally remarkable is the jump of the $\Delta(0)/(k_B T_c)$ ratio at p_c from values around 2.2, typical of ternary stannide superconductors at $p = 0$ [23] to values of about 3.7. All of these changes indicate the presence of a quantum critical point at $p_c \approx 1.6$ GPa, which, taking into account the uncertainties of a linear extrapolation, is close to the value which was postulated

from a linear extrapolation of the normal-state values of $T^*(p)$ to $T = 0$ [8]. Whereas part of the linear increase of $\lambda(0)^{-2}$ for $p < p_c$ can be related to the corresponding linear decrease of the mean free path of $\text{Ca}_3\text{Ir}_4\text{Sn}_{13}$ [8], the pronounced changes at and above p_c point to a profound modification of the electronic structure and of the superconducting interaction strength at p_c , and are a strong indication of the presence of a quantum critical point in the superconducting phase. Similar pressure measurements of $\text{Sr}_3\text{Ir}_4\text{Sn}_{13}$ for $0.15 < p < 2.5$ GPa, corresponding to values between -5.1 and -2.7 GPa of the $(\text{Ca}_{1-x}\text{Sr}_x)_3\text{Ir}_4\text{Sn}_{13}$ phase diagram, far away from p_c , do not exhibit pronounced or anomalous pressure effects [inset of Fig. 3(b)]. The total amplitude of the Gaussian signals of the μSR spectra, which is a measure of the volume fraction of the superconducting phase, does not show any pressure dependence and has the maximum possible value indicating a full volume superconducting phase below and above the quantum critical point.

III. DISCUSSION

A. Pressure dependence of superconducting parameters

The application of pressure allows one to uncover superconductivity and plays an important role in obtaining information about its microscopic mechanism. For instance, the dependence of T_c on pressure for MgB_2 indicated a mediating electron-phonon coupling [35]. Recently, in Bi_2Se_3 , an anomalously saturating p dependence of T_c (for $p > 30.0$ GPa) suggested the presence of an unconventional pressure-induced superconducting pairing state in this topological insulator [36], and pressure-induced reversal of the dependence of T_c on pressure in KFe_2As_2 indicated a pairing state transition [37]. Investigations have mainly focused on the study of $T_c(p)$ [38]. For the most simple metals and in the majority of the prototypical BCS superconductors, superconductivity is reduced under pressure $dT_c/dp < 0$. However, even in elementary superconductors, the effects of pressure can be complicated [39]. The variation of the critical temperature with pressure can be generically obtained by differentiating the McMillan expression for strongly coupled superconductors with respect to T_c [25,35,40],

$$\frac{d \ln T_c}{dp} = -(2A - 1) \frac{d \ln \omega_{\text{ln}}}{dp} + A \frac{d \ln \eta}{dp}, \quad (3)$$

where $A = 1.04\lambda_{\text{ep}}[1 + 0.38\mu^*]/[\lambda_{\text{ep}} - \mu^*(1 + 0.62\lambda_{\text{ep}})]^2$ is a function of the electron-phonon coupling constant λ_{ep} and of the Coulomb pseudopotential μ^* , ω_{ln} is the logarithmic-averaged phonon frequency, $\eta \equiv N(E_F)\langle I^2 \rangle$ is the Hopfield parameter with $\langle I^2 \rangle$ the electronic matrix element of the electron-phonon interaction averaged over the Fermi surface, and $N(E_F)$ is the density of states at the Fermi level.

To the pressure dependence of T_c , there are phononic and electronic contributions. In conventional phonon-mediated superconductors, the phonon stiffening with pressure leads to a decreasing critical temperature, although, close to a structural transition, phonon softening of particular modes can occur. For a BCS superconductor, the superfluid density and hence $\lambda(0)$ is pressure independent as well as the ratio $\Delta(0)/(k_B T_c)$. This is the case, for instance, of RbOs_2O_6 [25]. Also, in the

multigap superconductor MgB₂, which is a moderately strong electron-phonon-mediated superconductor, the two gap-to- T_c ratios are practically pressure independent and only a small pressure effect of $\lambda(0)$ has been observed [41]. No or small pressure dependence of $\lambda(0)^{-2}$ has been reported also in some unconventional superconductors, such as the electron-doped infinite-layer cuprate Sr_{0.9}La_{0.1}CuO₂ [42] or the nearly optimally hole-doped YBaCu₃O_{7- δ} [27].

In the (Ca_{1-x}Sr_x)₃Ir₄Sn₁₃ system, the positive variation of the critical temperature with pressure is a clear indication of the importance of the electronic contribution, such as a change of $N(E_F)$. The observed pressure-induced enhancement of the superfluid density is very high, with a relative variation between the lowest (0.15 GPa) and the highest (2.18 GPa) measured pressures $\Delta\lambda(0)^{-2}/\lambda(0)^{-2} \simeq 240\%$. This is unusual for a BCS superconductor.

B. Phase diagrams and Uemura plot

The pronounced increase setting in above 1.6 GPa can be understood if put it in relation to the structural quantum phase transition and the related CDW suppression at p_c . The superconducting and CDW gaps are often antagonistic toward each other. The CDW gapping inhibits superconductivity by decreasing the area of the Fermi surface where the superconducting gap can open and by reducing the number of available carriers. This is apparent in various physical properties of the (Ca_{1-x}Sr_x)₃Ir₄Sn₁₃ system. Optical spectroscopy measurements across the structural/CDW phase transition on single-crystal samples of Sr₃Ir₄Sn₁₃ have determined from the Drude components a reduction of the plasma frequency from $\omega_p \approx 30\,530\text{ cm}^{-1}$ above to $\omega_p \approx 25\,750\text{ cm}^{-1}$ below T^* [14]. If the effective mass of the itinerant carriers remains unchanged, this means that roughly 29% of the carriers are lost below T^* . In Ca₃Ir₄Sn₁₃, the temperature dependence of the Hall coefficient shows a significant reduction of carriers below T^* [13]. A reduction of the electronic density of states at E_F in the CDW phase has also been predicted by density functional theory (DFT) calculations of the electronic structure of Sr₃Ir₄Sn₁₃ [8,43].

Superconductivity in metallic ternary stannide compounds has been analyzed within the theory of strong-coupling superconductivity, where the gap can be expressed as a function of the logarithmic-averaged phonon frequency $\omega_{\text{ln}} \equiv \exp\left(\frac{2}{\lambda_{\text{ep}}} \int_0^\infty \ln \omega \alpha^2 F(\omega) d\ln \omega\right)$ and $x \equiv \frac{\omega_{\text{ln}}}{T_c}$,

$$\Delta(0)/k_B T_c = 1.768 \left[1 + \frac{12}{x^2} \ln \frac{x}{2} \right]. \quad (4)$$

For Sr₃Ir₄Sn₁₃ and Ca₃Ir₄Sn₁₃, specific-heat and magnetic susceptibility measurements yield $\omega_{\text{ln}} = 73$ and 56 K, respectively. The reduced values of ω_{ln} as compared to that of the Debye temperature ($\omega_D = 184$ and 218 K, respectively) indicate the importance of the low-energy phonon modes for the superconductivity in the ternary stannide compounds [23,24]. The pronounced increase of the gap-to- T_c ratio at p_c , however, cannot be simply understood within Eq. (4), which only predicts a maximum value for the ratio of 2.77, well below our observation [see Fig. 3(c)]. Since our data exclude the presence of spin fluctuations or magnetic glue at any pressure, it is natural to attribute the observed

effect to the particular role of phonons associated with the structural quantum phase transition and their synergetic effects with concomitant changes of the electronic spectrum related to the CDW suppression. The DFT calculations by Tompsett have identified low-energy phonon modes at the **X** and **M** points as responsible for the structural transition. A particular role appears to be played by the phonon mode at the **M** point, which corresponds to a breathing of the Sn₁₂ cages [43]. These phonon modes go soft at T^* . Softening of a low-energy phonon mode associated with the Sn₁₂ breathing mode has also been found by inelastic neutron scattering [10]. When the transition temperature is driven to 0 K by pressure, the softening occurs at this temperature, giving rise to additional low-lying phonon modes, which can be excited at low temperatures. The effect of these additional phonon modes on the superconducting strength can be estimated using a model originally proposed for the fullerenes, which takes into account electron coupling to phonons with very large differences in frequency [44]. Such a model is able to produce a gap-to- T_c ratio of 5, well encompassing the observed increase to ~ 3.7 at p_c , and is able to explain the transition from intermediate strong to very strong superconductivity at pressures $p > p_c$ [44]. This result suggests that the low-energy phonons are not only responsible for the structural transition, but also drive and boost the competing superconducting phase, which reaches its maximum T_c at ~ 4.0 GPa. A similar mechanism could be at the origin of the superconducting dome in the CDW superconductor 1T-TiSe₂ when the CDW transition is suppressed by pressure within a behavior also reminiscent of a quantum critical point [45]. However, we cannot exclude that a role may also be played by charge density fluctuations on approaching the QCP.

The pronounced increase of ρ_s and $\Delta(0)/(k_B T_c)$ when T^* is driven to zero clearly indicates that below p_c , the CDW gap is competing with the superconducting gap and that only its complete suppression allows superconductivity to fully develop. However, from the amplitude of the μ SR signal, we can deduce that while competing for the same electrons, the two order parameters coexist at nanoscale with the superconducting volume fraction remaining 100% over the entire pressure range. Overall, our results indicate that the (Ca_{1-x}Sr_x)₃Ir₄Sn₁₃ system has a quantum critical point at ≈ 1.6 GPa, separating two different superconducting states, i.e., a low-pressure one coexisting with a CDW and a pure-superconducting one at higher pressures, resulting in a phase diagram as shown in Fig. 4.

From the data, we can also estimate the increase of available carriers associated with the closing of the CDW gap. As a measure, we take the relative difference between $\lambda(0)^{-2}$ of Ca₃Ir₄Sn₁₃ at 1.16 GPa, where superconductivity is coexisting with the CDW phase at all temperatures, and $\lambda(0)^{-2}$ at 2.18 GPa, where the CDW is completely suppressed. The relative increase in superfluid density is 68(4)%. DFT calculations of the electronic structure of Sr₃Ir₄Sn₁₃ with the generalized gradient approximation (GGA) have predicted a $\sim 34\%$ increase of $N(E_F)$ when raising the temperature above T^* [8]. Within the simplified assumption of a free-electron gas model, where $N(E_F) \propto n^{-1/3}$, this corresponds to a $\sim 140\%$ increase of charge carriers. This number appears reasonable if one takes into account that changes in $\lambda(0)^{-2}$ also reflect changes of the effective mass $m^* = m_b(1 + \lambda_{\text{int}})$, which we

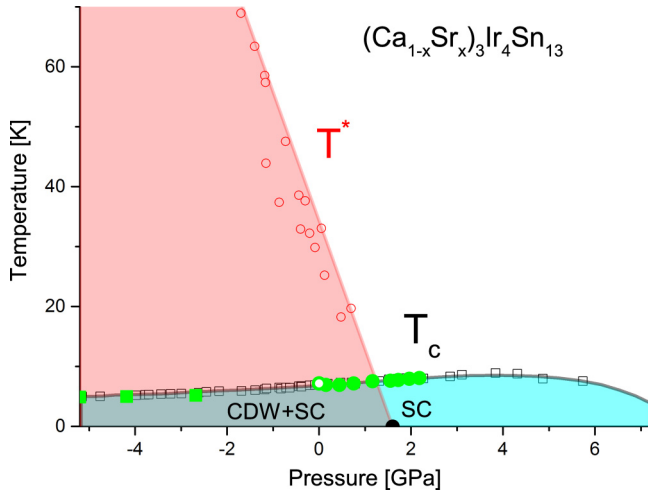


FIG. 4. (Color online) Low-temperature phase diagram of $(\text{Ca}_{1-x}\text{Sr}_x)_3\text{Ir}_4\text{Sn}_{13}$ proposed by the present μSR investigations of the microscopic superconducting parameters. They indicate that there are two superconducting phases, i.e., one coexisting with CDW and the other pure. They are separated by a critical point at ≈ 1.6 GPa, indicated by a black dot. Green circles and squares are the superconducting transition temperatures of $\text{Ca}_3\text{Ir}_4\text{Sn}_{13}$ and $\text{Sr}_3\text{Ir}_4\text{Sn}_{13}$ under pressure obtained from the μSR data. The open green circle is a point at $p = 0$ from [22]. The open squares are T_c values from ac susceptibility and resistivity measurements and open circles are T^* values from resistivity measurements; data from Ref. [8].

may expect to increase by entering the very strong-coupling regime above p_c .

The difference by almost a factor of two of the gap amplitudes in the two superconducting phases is in agreement with the dependence of the BCS ratio on the CDW gap and the degree of Fermi-surface gapping as calculated in [46], where it was shown that the electron-hole gapping in the CDW-superconducting phase may lead to a reduction of the BCS ratio by as much as one half. Our data also show that while the gap amplitude $\Delta(0)$ strongly depends on the suppression of the CDW, the temperature dependence of the original BCS expression is not affected by the presence of the CDW and is independent of the coupling strength. On the other hand, a comparison of Fig. 3(a) with Figs. 3(b) and 3(c) shows that T_c is much less sensitive to the quantum critical point than the superfluid density and the coupling strength. This reflects the fact that whereas closing the CDW gap makes electronic states at the Fermi surface available for superconductivity and directly increases n_s , the electronic contribution to $d\ln T_c/dp$ as expressed by Eq. (3) only depends logarithmically on $N(E_F)$.

Whereas BCS superconductors did not show any pressure effects on the superfluid density, more or less pronounced effects have been observed in unconventional superconductors. In layered cuprates, in the presence of charge reservoir layers, pressure-induced charge transfer to the CuO_2 planes is an important mechanism besides changes of the effective pairing interaction to increase ρ_s . A large transfer of holes from the double chains to the CuO_2 planes has been observed in $\text{YBa}_2\text{Cu}_4\text{O}_8$, which also displays a large pressure derivative of T_c and large increase of superfluid density $\frac{\Delta[\lambda(0)^{-2}]}{\lambda(0)^{-2}} = 42\%$ at

1.0 GPa pressure. Here, however, about two-thirds of the effect has been attributed to a reduction of the effective mass [26]. Pronounced pressure dependence of ρ_s or pressure-induced superconductivity has been often found in unconventional systems with magnetic phases and where magnetic fluctuations are the most probable candidates for an attractive interaction. Examples are (pressure-induced) superconductivity in the antiferromagnetic phase of the noncentrosymmetric heavy-fermion CeRhSi_3 [47], in the ferromagnetic phase of UGe_2 [48]. In the prototypical heavy-fermion superconductor CeCoIn_5 , the increase of ρ_s under pressure corresponds to about a doubling of the supercarrier number density n_s between 0 and 1.0 GPa. The (smooth) increase was related to the possible presence of a quantum critical point [49].

The phase diagram of $(\text{Ca}_{1-x}\text{Sr}_x)_3\text{Ir}_4\text{Sn}_{13}$ reminiscent of unconventional superconductors, the pronounced pressure dependence of ρ_s , and the jump of gap and coupling strength at the quantum critical point raise the question about a possible unconventional character of this compound. Unconventional superconductivity is often found in strongly correlated electron systems, displays order parameter with gaps which are anisotropic and displaying sign reversal between different Fermi-surface pockets, or is related to intrinsic magnetism, connected to competing magnetic phases or displaying broken symmetries, such as inversion or time-reversal symmetry. None of these characteristics is found in this system, which has an s -wave order parameter all over the phase diagram and attractive interaction where phonons appear to play a dominant role.

$\text{Ca}_3\text{Ir}_4\text{Sn}_{13}$ appears to have moderately heavy carriers and weak correlation [12,13]. The dimensionless ratio of the thermopower (Seebeck coefficient) S/T to the specific-heat term $q = \frac{N_{Av}eS}{T\gamma}$, provided a carrier density $|q^{-1}| \cong 11.8(8)$ per f.u., corresponding to high density of states (DOS) per volume [13]. Note that from the Sommerfeld coefficient for $\text{Ca}_3\text{Ir}_4\text{Sn}_{13}$ $\gamma_{\text{meas}} = 39 \text{ mJ/K}^2 \text{ mol}$ [13], we get a similar carrier density $n_e = 5.3 \times 10^{22} \text{ cm}^{-3}$, which gives a BCS coherence length $\xi_0 = \hbar^2(3\pi^2n_e)^{1/3}/[m_e(1+\lambda_{\text{ep}})\pi\Delta(0)] \sim 80 \text{ nm}$ (where we used for the electron-phonon coupling $\lambda_{\text{ep}} = 1.34$, from [24], and $\Delta(0) = 1.51 \text{ meV}$). Using the value of the residual resistivity above T_c ($\rho_n = 79 \mu\Omega \text{ cm}$), we estimate the mean free path $\ell = \hbar(3\pi^2)^{1/3}/(n_e^{2/3}\rho_n e^2) = 1.14 \text{ nm} \ll \xi_0$. The dirty character of the superconductor is consistent with our analysis of $\lambda(T)$.

The effective coherence length obtained from $B_{c2}(0) = 5.4 \text{ T}$, determined from the well-known Werthamer-Helfand-Hohenberg (WHH) formula $B_{c2}(0) = -0.693 T_c \frac{dB_{c2}}{dT}$, is $\xi_{\text{GL}} = \sqrt{\frac{\Phi_0}{2\pi B_{c2}}} \cong 7.8 \text{ nm}$, where $\Phi_0 = 2.07 \times 10^{-15} \text{ T m}^2$ is the quantum of magnetic flux. The good agreement of ξ_{GL} with the value obtained from $\sqrt{\xi_0 \ell} \cong 9.5 \text{ nm}$ gives us further confidence about the correct estimate of these electronic parameters. The low value of $\ell/\xi_0 = 0.014$ means that in $\text{Ca}_3\text{Ir}_4\text{Sn}_{13}$, the density of paired electrons is reduced to $n_s \approx n_e \frac{\ell}{\xi_0} = 7.4 \times 10^{20} \text{ cm}^{-3}$. From our determination of the effective magnetic penetration depth λ , we can alternatively estimate the density of paired electrons to be $n_s = \frac{m_e(1+\lambda_{\text{ep}})}{\mu_0 e^2 \lambda^2} \cong 5.36 \times 10^{20} \text{ cm}^{-3}$. This number is in good agreement with the above estimate, which is based on a carrier density expressed

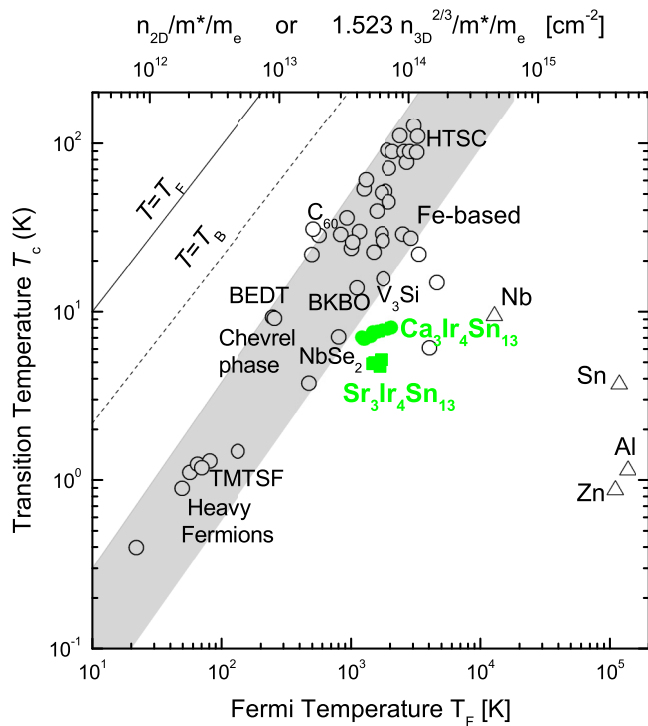


FIG. 5. (Color online) Uemura plot. Green points: The superconducting transition temperature T_c vs the effective Fermi temperature T_F for $\text{Ca}_3\text{Ir}_4\text{Sn}_{13}$ and $\text{Sr}_3\text{Ir}_4\text{Sn}_{13}$ at various pressures. The points are plotted in the $T_c - T_F$ diagram together with data of different families of superconductors (plot adapted from [50,52]). Top scale: T_F expressed in terms of paired carrier density and effective mass, evaluated from the $\lambda(0)^{-2}$ measurements, i.e., $1.52 n_s^{2/3}/m_e^*$ for a three-dimensional (3D) system such as $(\text{Ca}_{1-x}\text{Sr}_x)_3\text{Ir}_4\text{Sn}_{13}$ and n_s/m_e^* for 2D systems. The unconventional superconductors are generally considered to fall within a band, indicated by the gray region in the figure. Conventional elemental superconductors lie on the right side of the diagram. The dashed line corresponds to the Bose-Einstein condensation temperature T_B .

in terms of a simple free-electron model, and reconfirms the applicability of the BCS theory.

To place $(\text{Ca}_{1-x}\text{Sr}_x)_3\text{Ir}_4\text{Sn}_{13}$ in the context of other superconductors, we plot in Fig. 5 the measured points in the Uemura graph of T_c versus effective Fermi temperature, which is often used to define the character of unconventional superconductors [50,51]. The green symbols correspond to different pressures for $\text{Ca}_3\text{Ir}_4\text{Sn}_{13}$ studied here, and the other points are taken from [50,52]. Remarkably, plotting the values of T_c as a function of the effective Fermi temperature, which for a 3D system is $k_B T_F = \frac{\hbar^2}{2} (3\pi^2)^{2/3} \frac{n_s^{2/3}}{m_e^*}$, where n_s is the value determined above from λ , we observe that $\text{Ca}_3\text{Ir}_4\text{Sn}_{13}$ lies at the border of that part of the diagram where cuprates and iron-based superconductors and other unconventional superconductors are found. A similar result is obtained if we express the superfluid density in term of the muon spin-relaxation rate $\sigma(0) \propto \lambda(0)^{-2} \propto \rho_s(0)$ as in the original Uemura plot. This behavior shows that a conventional electron-phonon-mediated cubic superconductor is not a criterium of exclusion from this part of the plot. The vicinity to unconventional superconductors is possibly related to the competing CDW state or to the presence of a quantum phase transition. Remarkably, the investigated system is placed in the Uemura plot close to V_3Si , another phonon-mediated superconductor with a nearby structural instability.

Recently, it was reported that the series $(\text{Ca}_{1-x}\text{Sr}_x)_3\text{Rh}_4\text{Sn}_{13}$ has a very similar phase diagram with a quantum critical point, which should appear at ambient pressure if the Ca fraction is 0.9 [15]. This opens the possibility to study the interplay of superconductivity, CDW, and quantum criticality over a broader interval of pressures even beyond the region where superconductivity is strongest and the critical temperature reaches its maximum.

Note added. Recently, strong-coupling superconductivity was also reported near a structural quantum critical point of $(\text{Ca}_{1-x}\text{Sr}_x)_3\text{Rh}_4\text{Sn}_{13}$ [53].

ACKNOWLEDGMENTS

Work at PSI was supported by the Swiss National Science Foundation. Work at Brookhaven National Laboratory is supported by the U.S. Department of Energy under Contract No. DE-SC00112704.

- [1] B. Keimer, S. A. Kivelson, M. R. Norman, S. Uchida, and J. Zaanen, *Nature (London)* **518**, 179 (2015).
- [2] J. Paglione and R. L. Greene, *Nat. Phys.* **6**, 645 (2010).
- [3] D. J. Scalapino, *Rev. Mod. Phys.* **84**, 1383 (2012).
- [4] E. Fradkin, S. A. Kivelson, and J. M. Tranquada, *Rev. Mod. Phys.* **87**, 457 (2015).
- [5] P. Coleman and A. J. Schofield, *Nature (London)* **433**, 226 (2005).
- [6] J. Remeika, G. S. Espinosa, A. S. Cooper, H. Barz, J. M. Rowell, D. B. McWhan, J. M. Vandenberg, D. E. Moncton, Z. Fisk, L. D. Woolf, H. C. Hamaker, M. B. Maple, G. Shirane, and W. Thomlinson, *Solid State Commun.* **34**, 923 (1980).
- [7] G. P. Espinosa, *Mater. Res. Bull.* **15**, 791 (1980).
- [8] L. E. Klintberg, S. K. Goh, P. L. Alireza, P. J. Saines, D. A. Tompsett, P. W. Logg, J. Yang, B. Chen, K. Yoshimura, and F. M. Grosche, *Phys. Rev. Lett.* **109**, 237008 (2012).
- [9] S. Y. Zhou, H. Zhang, X. C. Hong, B. Y. Pan, X. Qiu, W. N. Dong, X. L. Li, and S. Y. Li, *Phys. Rev. B* **86**, 064504 (2012).
- [10] D. G. Mazzone, J. L. Gavilano, R. Sibille, M. Medarde, B. Delley *et al.*, *Phys. Rev. B* **92**, 024101 (2015).
- [11] C. N. Kuo, H. F. Liu, C. S. Lue, L. M. Wang, C. C. Chen, and Y. K. Kuo, *Phys. Rev. B* **89**, 094520 (2014).
- [12] L. M. Wang, C. Y. Wang, G. M. Chen, C. N. Kuo, and C. S. Lue, *New J. Phys.* **17**, 033005 (2015).
- [13] K. Wang and C. Petrovic, *Phys. Rev. B* **86**, 024522 (2012).
- [14] A. F. Fang, X. B. Wang, P. Zheng, and N. L. Wang, *Phys. Rev. B* **90**, 035115 (2014).

- [15] S. K. Goh, D. A. Tompsett, P. J. Saines, H. C. Chang, T. Matsumoto, M. Imai, K. Yoshimura, and F. M. Grosche, *Phys. Rev. Lett.* **114**, 097002 (2015).
- [16] C. N. Kuo, C. W. Tseng, C. M. Wang, C. Y. Wang, Y. R. Chen, L. M. Wang, C. F. Lin, K. K. Wu, Y. K. Kuo, and C. S. Lue, *Phys. Rev. B* **91**, 165141 (2015).
- [17] W. Tabis, Y. Li, M. Le Tacon, L. Braicovich, A. Kreyssig *et al.*, *Nat. Commun.* **5**, 5875 (2014).
- [18] J. Chang *et al.*, *Nat. Phys.* **8**, 871 (2012).
- [19] J. Yang, B. Chen, C. Michioka, and K. Yoshimura, *J. Phys. Soc. Jpn.* **79**, 113705 (2010).
- [20] S. Gerber, J. L. Gavilano, M. Medarde, V. Pomjakushin, C. Baines, E. Pomjakushina, K. Conder, and M. Kenzelmann, *Phys. Rev. B* **88**, 104505 (2013).
- [21] P. K. Biswas, A. Amato, R. Khasanov, H. Luetkens, Kefeng Wang, C. Petrovic, R. M. Cook, M. R. Lees, and E. Morenzoni, *Phys. Rev. B* **90**, 144505 (2014).
- [22] P. K. Biswas, A. Amato, Kefeng Wang, C. Petrovic, R. Khasanov, H. Luetkens, and E. Morenzoni, *J. Phys.: Conf. Ser.* **551**, 012029 (2014).
- [23] N. Kase, H. Hayamizu, and J. Akimitsu, *Phys. Rev. B* **83**, 184509 (2011).
- [24] H. Hayamizu, N. Kase, and J. Akimitsu, *J. Phys. Soc. Jpn.* **80**, SA114 (2011).
- [25] R. Khasanov, D. G. Eshchenko, J. Karpinski, S. M. Kazakov, N. D. Zhigadlo, R. Brütsch, D. Gavillet, D. Di Castro, A. Shengelaya, F. La Mattina, A. Maisuradze, C. Baines, and H. Keller, *Phys. Rev. Lett.* **93**, 157004 (2004).
- [26] R. Khasanov, J. Karpinski, and H. Keller, *J. Phys. Condens. Mater.* **17**, 2453 (2005).
- [27] A. Maisuradze, A. Shengelaya, A. Amato, E. Pomjakushina, and H. Keller, *Phys. Rev. B* **84**, 184523 (2011).
- [28] See Supplemental Material at <http://link.aps.org/supplemental/10.1103/PhysRevB.92.195122> for details on data analysis.
- [29] E. H. Brandt, *Phys. Rev. B* **68**, 054506 (2003).
- [30] S. K. Goh, L. E. Klintberg, P. L. Alireza, D. A. Tompsett, J. Yang, B. Chen, K. Yoshimura, and F. M. Grosche, [arXiv:1105.3941v1](https://arxiv.org/abs/1105.3941v1).
- [31] M. Tinkham, *Introduction to Superconductivity*, 2nd ed. (Dover, New York, 2004).
- [32] B. Mühlischlegel, *Z. Phys.* **155**, 313 (1959).
- [33] A. Carrington and F. Manzano, *Physica C* **385**, 205 (2003).
- [34] H. Padamsee, and J. E. Neighbor, and C. A. Shiffman, *J. Low Temp. Phys.* **12**, 387 (1973).
- [35] T. Tomita, J. J. Hamlin, J. S. Schilling, D. G. Hinks, and J. D. Jorgensen, *Phys. Rev. B* **64**, 092505 (2001).
- [36] K. Kirshenbaum, P. S. Syers, A. P. Hope, N. P. Butch, J. R. Jeffries, S. T. Weir, J. J. Hamlin, M. B. Maple, Y. K. Vohra, and J. Paglione, *Phys. Rev. Lett.* **111**, 087001 (2013).
- [37] F. F. Tafti, J. P. Clancy, M. Lapointe-Major, C. Collignon, S. Faucher *et al.*, *Phys. Rev. B* **89**, 134502 (2014).
- [38] J. S. Schilling, *Frontiers of High Pressure Research II: Application of High Pressure to Low-Dimensional Novel Electronic Materials*, Vol. 48 of NATO Science Series (Springer, Berlin, 2001), pp. 345–360.
- [39] C. Buzea and K. Robbie, *Supercond. Sci. Tech.* **18**, R1 (2005).
- [40] W. L. McMillan, *Phys. Rev.* **167**, 331, (1968); B. Allen and R. C. Dynes, *Phys. Rev. B* **12**, 905 (1975).
- [41] D. Di Castro, R. Khasanov, C. Grimaldi, J. Karpinski, S. M. Kazakov, R. Brutsch, and H. Keller, *Phys. Rev. B* **72**, 094504 (2005).
- [42] D. Di Castro, R. Khasanov, A. Shengelaya, K. Conder, D. J. Jang, M. S. Park, S. I. Lee, and H. Keller, *J. Phys. Condens. Mater.* **21**, 275701 (2009).
- [43] D. A. Tompsett, *Phys. Rev. B* **89**, 075117 (2014).
- [44] I. I. Mazin, O. V. Dolgov, A. Golubov, and S. V. Shulga, *Phys. Rev. B* **47**, 538 (1993).
- [45] A. F. Kusmartseva, B. Sipoš, H. Berger, L. Forro, and E. Tutis, *Phys. Rev. Lett.* **103**, 236401 (2009).
- [46] A. M. Gabovich, A. I. Voitenko, and M. Ausloos, *Phys. Rep.* **367**, 583 (2002), and references therein.
- [47] N. Kimura, K. Ito, K. Saitoh, Y. Umeda, H. Aoki, and T. Terashima, *Phys. Rev. Lett.* **95**, 247004 (2005).
- [48] S. S. Saxena, P. Agarwal, K. Ahilan, F. M. Grosche, R. K. W. Haselwimmer, M. J. Steiner, E. Pugh, I. R. Walker, S. R. Julian, P. Monthoux, G. G. Lonzarich, A. Huxley, I. Sheikin, D. Braithwaite, and J. Flouquet, *Nature (London)* **406**, 587 (2000).
- [49] L. Howald, A. Maisuradze, P. D. de Reotier, A. Yaouanc, C. Baines, G. Lapertot, K. Mony, J. P. Brison, and H. Keller, *Phys. Rev. Lett.* **110**, 017005 (2013).
- [50] K. Hashimoto, K. Cho, T. Shibauchi, S. Kasahara, Y. Mizukami, R. Katsumata, Y. Tsuruhara, T. Terashima, H. Ikeda, M. A. Tanatar, H. Kitano, N. Salovich, R. W. Giannetta, P. Walmsley, A. Carrington, R. Prozorov, and Y. Matsuda, *Science* **336**, 1554 (2012).
- [51] Y. J. Uemura, *J. Phys. Condens. Mater.* **16**, S4515 (2004).
- [52] R. Khasanov, H. Luetkens, A. Amato, H.-H. Klauss, Z.-A. Ren, J. Yang, W. Lu, and Z.-X. Zhao, *Phys. Rev. B* **78**, 092506 (2008).
- [53] W. C. Yu, Y. W. Cheung, P. J. Saines, M. Imai, T. Matsumoto, C. Michioka, K. Yoshimura, and S. K. Goh, *Phys. Rev. Lett.* **115**, 207003 (2015).